Taylor & Francis
Taylor & Francis Group

Combustion Theory and Modelling

ISSN: 1364-7830 (Print) 1741-3559 (Online) Journal homepage: http://www.tandfonline.com/loi/tctm20

The effect of damköhler number on the stand-off distance of cross-flow flames

Matthew Juniper & Sébastien Candel

To cite this article: Matthew Juniper & Sébastien Candel (2003) The effect of damköhler number on the stand-off distance of cross-flow flames, Combustion Theory and Modelling, 7:3, 563-577, DOI: 10.1088/1364-7830/7/3/307

To link to this article: http://dx.doi.org/10.1088/1364-7830/7/3/307

INSTITUTE OF PHYSICS PUBLISHING COMBUSTION THEORY AND MODELLING

Combust. Theory Modelling **7** (2003) 563–577 PII: S1364-7830(03)58758-7

The effect of Damköhler number on the stand-off distance of cross-flow flames

Matthew Juniper and Sébastien Candel

Laboratoire EM2C, Ecole Centrale de Paris, Grande Voie des Vignes, Châtenay-Malabry, Cedex, France

Received 24 January 2003, in final form 28 July 2003
Published 1 September 2003
Online at stacks.iop.org/CTM/7/563

Abstract

Cross-flow flames, formed between two reactants approaching at 90°, have many similarities to edge flames formed between parallel-flowing reactants. Two types can be distinguished: one whose inlet velocity profiles have a uniform strain rate and another whose inlet velocity profile is flat. Dimensional analysis suggests that the distance between the flame head and the confluence point, L_c, is affected by a Damköhler number. A simplified solution for the relationship between the non-dimensional stand-off distance Π and the Damköhler number is determined here by correlating the results of several hundred numerical simulations. For a cross-flow flame that is controlled by the strain rate, it is found that $L_c \propto A\,\mathcal{D}^{1/2}\,\tau_c^{1/2}$, where A is the strain rate, $\mathcal{D}$ is the diffusivity and τ_c is the chemical time. For a convection-controlled flame, the expression is: $L_c \propto U^3\,\tau_c^2\,\mathcal{D}^{-1}$, where U is the entry velocity.

1. Introduction

Analysis of generic configurations has been very useful for the advancement of combustion theory. The cross-flow flame is one such case, where much can be learned about flame stabilization. These flames are formed between two reactant streams which impinge at 90°, as shown in figure 1. Oxidizer flows through the bottom boundary while the fuel is injected through the left boundary. Cross-flow flames are similar to edge flames, figure 2, which form behind thin splitter plates separating two co-flowing streams. Both cross-flow flames and edge flames are the fronts of diffusion flames which are propagating into non-premixed or stratified fresh gases. However, their behaviour is subtly different, as this article demonstrates.

The cross-flow flame has recently been introduced to the field of combustion [1] and currently there is little work on this subject. However, there has been extensive work on edge flames. A review of edge flames, comprising experimental, analytical and numerical approaches, can be found in [2]. Analytical models of edge flames require great simplification because the flows are relatively complicated. Examples of such approaches can be found in the early analysis of [3] and in more recent studies such as those of [4–6]. The presence of

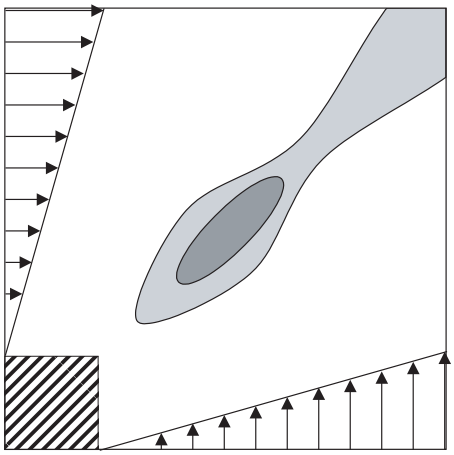

Figure 1. A cross-flow flame is formed between two non-premixed reactant streams impinging at 90°.

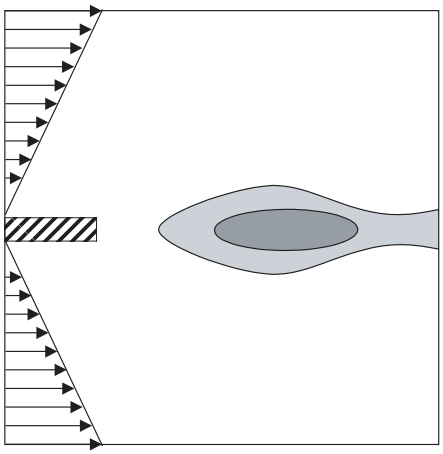

Figure 2. An edge flame is formed between two non-premixed reactant streams which are initially parallel.

a thick splitter plate between the reactant streams leads to even greater complexity and has been tackled by [7, 8]. A useful numerical approach is given in [9].

If there is a reasonably high degree of pre-mixing in front of an edge flame, a triple flame forms, featuring two premixed lateral branches and a central diffusion flame. When there is less pre-mixing in front of the flame, the triple flame loses its lean and rich arms to become a reaction kernel. In the kernel, the volumetric reaction rate is significantly greater than that characterizing the diffusion flame that trails behind it. When there is very little pre-mixing, for example, where preheated reactants meet behind a splitter plate, a diffusion flame forms instantly and there is no discernable edge. Similar behaviour is found for cross-flow flames.

Cross-flow flames form between two reactants which approach at 90°. By convention, these reactants flow perpendicular to the x and y axes. A flame head propagates into the pre-mixed region near the origin, trailing a diffusion flame along the line $y = x$. Two distinct cases can immediately be identified, characterized by the shape of the inlet velocity profiles.

The situation studied in [1] has velocity profiles with constant strain rate, A, such that $u = Ay$ along the y axis and $v = Ax$ along the x-axis. This is equivalent to a stagnation point potential flow with the axes rotated by 45°. In this paper, this situation is known as 'strain rate controlled' because the flame head is situated in a region of high strain. An alternative configuration has flat inlet velocity profiles and a more complex velocity field. Numerical simulations in cold flow demonstrate that the velocity along the line $y = x$ tends to a constant value and this situation is known as 'convection controlled'. Edge flames can also be strain rate controlled [9] or convection controlled [3].

In practical situations, cross-flow flames can be formed when one reactant is blown through a porous plate into a perpendicular stream of another reactant [10]. This situation is similar to the flame stationed in a convecting stream above a vaporizing fuel, a classic problem in combustion theory [11]. This problem is discovered repeatedly in practical studies of flame spread [12], of the combustion of grains of solid rocket fuel [13] and in flame stabilization inside liquid-fuelled rocket motors [14]. In many of these cases, one or both of the reactant streams has a boundary layer velocity profile. If the flame head is situated well within this boundary layer, it will tend to be strain rate controlled. Otherwise, it will tend to be convection controlled. The factors affecting the distance between the flame head and the confluence point determine whether or not a flame is stabilized. Conventional approaches to this problem [15] cannot model the flame tip, hence the motivation for this study.

The aim is more precisely to develop dimensionless parameters that determine the flame stand-off distance for both types of cross-flow flames. There are three such parameters and the influence of one of them, a Damköhler number, is studied in detail. A numerical method is used which is reminiscent of the experimental studies employed to develop a simplified solution from the results of a dimensional analysis. This yields simple relationships for the flame stand-off distances of both types of cross-flow flames. It does not explain why these relationships exist, although these reasons can be deduced to some extent from the tendencies observed. Dimensional analysis combined with systematic calculations constitutes a practical approach which can be easily extended to examine other parameters. Furthermore, the expressions developed can be compared with complete solutions currently being derived from theoretical arguments [17].

In section 2, dimensional analysis is applied to cross-flow flames in order to highlight the key parameters of the problem. These parameters are very similar to those found for edge flames, so a review of dimensionless analysis of edge flames is presented in section 3. This section is not placed in the introduction because it relies on concepts introduced in section 2. The effect of Damköhler number on cross-flow flames is determined in section 4.

2. Problem formulation and dimensional analysis of cross-flow flames

Governing equations for mass, momentum, energy and species are:

$$\frac{\partial \rho}{\partial t} + \frac{\partial(\rho v_j)}{\partial x_j} = 0 \tag{1}$$

$$\frac{\partial(\rho v_i)}{\partial t} + \frac{\partial(\rho v_i v_j)}{\partial x_j} = -\frac{\partial p}{\partial x_i} + \frac{\partial \tau_{ij}}{\partial x_j} \tag{2}$$

$$\frac{\partial(\rho e_t)}{\partial t} + \frac{\partial(\rho h_t v_j)}{\partial x_j} = -\frac{\partial q_j}{\partial x_j} + \frac{\partial(\tau_{ij} v_i)}{\partial x_j} + \dot{w}_T \tag{3}$$

$$\frac{\partial(\rho Y_k)}{\partial t} + \frac{\partial(\rho Y_k v_j)}{\partial x_j} = -\frac{\partial(\rho Y_k V_{k,j}^D)}{\partial x_j} + \dot{w}_k \qquad k = O, F. \tag{4}$$

In these equations ρ, v_j, p, Y_k, e_t and h_t respectively designate the density, velocity components, pressure and mass fractions, total energy $e_t = e + \frac{1}{2}v_j v_j$ and total enthalpy $h_t = e_t + p/\rho$. The viscous stress tensor τ_{ij}, the heat flux vector q_j and the diffusion velocity vector are described by Newton, Fourier and Fick's models:

$$\tau_{ij} = \mu\left(\frac{\partial v_j}{\partial x_i} + \frac{\partial v_i}{\partial x_j} - \frac{2}{3}\delta_{ij}\frac{\partial v_l}{\partial x_j}\right) \tag{5}$$

$$q_j = -\lambda\frac{\partial T}{\partial x_j} \tag{6}$$

$$V_{k,j}^D = -D_k\frac{\partial Y_k}{\partial x_j}. \tag{7}$$

In the fully compressible case the density, temperature and pressure are related by the perfect gas law while in the thermodiffusive approximation this equation is replaced by a constant density assumption. The reaction rates in the energy and mass fraction equations are related to the reaction rate $\dot{w}_T = \dot{w}Q$, $\dot{w}_F = -\nu_F W_F \dot{w}$, $\dot{w}_O = -\nu_O W_O \dot{w}$ where Q, W_O, W_F are the heat released by the reaction and the molar masses of oxidizer and fuel. The chemical reaction is modelled as a single step $\nu_F F + \nu_O O \rightarrow \nu_P P$ with Arrhenius rate $\dot{w} = B\exp(-T_a/T)$.

These governing equations are solved by the numerical platforms introduced in section 4.1. Initially, however, dimensional analysis is used to highlight the key parameters of the problem and provide scaling laws for further comparison with theoretical, numerical or experimental results. In dimensional analysis, it is assumed that one can list all the dimensional variables affecting a system. This requires intuition similar to that required to construct a theoretical model of the system. These variables are then combined into dimensionless groups which can be used either to correlate data or as a basis for rational scaling of the system. There are some pitfalls to this approach, as is pointed out in [18]. For instance, one can generate dimensionless groups that have little or no effect. This may pass unnoticed if the inferences are not tested experimentally. Furthermore, even if extensive experiments are carried out, false correlations can appear due to the presence of a dimensional variable in more than one dimensionless group.

It is evident that dimensional analysis will be most successful when applied to simple configurations, where the complete set of variables affecting the system can be listed with confidence. In a simple case, the number of dimensionless parameters must be small and the discovery of the relationship between them is usually attempted by experiments. However, it is often difficult to devise an experiment that eliminates every variable except those in the simple configuration and this can lead to false results.

A numerical approach is particularly suitable as a replacement for experiments. It is easy, indeed preferable, to study only a simple problem and to eliminate all superfluous variables. A series of tests can be performed over a wide range of operating conditions and with small increments in the variables. This tends to the ideal method of performing dimensional analysis which is proposed in the conclusions of [18]. The only constraint is the speed of the numerical code, which must enable large numbers of simulations to be performed in a reasonable time span. By this method, the relationship between the small number of dimensional parameters can be deduced.

Even the simple configuration of a cross-flow flame contains dozens of potentially influential parameters. This is also true for edge flames. It is necessary to eliminate several at the outset by declaring that they shall not be varied. Such variables include the specific heat capacity, the molecular mass and the pressure. Furthermore, the molecular transport properties can be linked by fixing the Lewis and Prandtl numbers at unity. For a single step Arrhenius-rate reaction, this leaves seven variables, shown in table 1. The flame stand-off distance, for which

Table 1. Independent variables controlling the shape of a cross-flow flame.

Symbol	Description	Units
$\mathcal{D}$	Mass diffusivity	$m^2\ s^{-1}$
T_{in}	Reactant inlet temperature	K
T_f	Adiabatic flame temperature	K
T_a	Activation temperature of Arrhenius expression	K
B	Pre-exponential factor of Arrhenius expression	varies
τ_c	A chemical time appearing in the Arrhenius expression	s
L_c	Flame stand-off distance	m
Either A	Strain rate in strain-rate-controlled flame	s^{-1}
or U	Entry velocity in convection-controlled flame	ms^{-1}

we aim to develop a simplified solution, is defined as the distance between the origin and the point of maximum heat release.

There are seven variables and three dimensions. This suggests that the situation can be described entirely by four dimensionless groups, the first three of which are familiar to combustion theorists:

- The first is the Zeldovich number, given by $Ze \equiv T_a(T_f - T_{in})/T_{in}^2$ or occasionally $Ze \equiv T_a(T_f - T_{in})/T_f^2$. It is a measure of the activation energy.
- The second is a heat release parameter, given by $\alpha \equiv (T_f - T_{in})/T_f$.
- The third is a Damköhler number, obtained from the ratio of the characteristic chemical time to another characteristic time, which depends on whether the situation is strain rate controlled or convection controlled.
  - (a) A characteristic time of the strain rate is given by A^{-1}, leading to a strain rate Damköhler number: $\mathrm{Da}_1 \equiv \mathrm{A}^{-1/2}\,\tau_\mathrm{c}^{-1/2}$.
  - (b) A characteristic convection time is given by $L_{ref}U^{-1}$. The only characteristic length that is independent of the velocity field is given by the flame itself, which has thickness $L_{ref} = \delta_f \sim \tau_c^{1/2}\,\mathcal{D}^{1/2}$. U is the free stream inlet velocity and $\mathcal{D}$ is the diffusivity. This leads to a convection Damköhler number: $\mathrm{Da}_2 \equiv \mathcal{D}^{1/2}\,\mathrm{U}^{-1}\,\tau_\mathrm{c}^{-1/2}$.
- The fourth parameter is the ratio of the flame stand-off distance to the flame thickness: $\Pi \equiv L_c\,\tau_c^{-1/2}\,\mathcal{D}^{-1/2}$

There are several ways to define the characteristic chemical time τ_c. The processes to be investigated here concern a balance between flow and ignition, which suggests that the ignition time of a well-stirred mixture could be pertinent:

$$\tau_i = \frac{T_{in}}{T_a}\,\frac{c_v T_{in}}{qB\rho}\,\left(\frac{W_F W_O}{Y_{F_0} Y_{O_0}}\right)\,\exp\left(\frac{T_a}{T_{in}}\right) \tag{8}$$

The constant volume heat capacity is given by c_v; q represents the heat release of reaction per mass of fuel; W and Y represent molar masses and mass fractions respectively. Subscripts F and O refer to fuel and oxidizer. On inspection, one can determine dependence on: T_a/T_{in}, which is akin to the Zeldovich number; $c_v T_{in}/q$, which is a heat release parameter and the inverse pre-exponential factor B^{-1}. In the study of cross-flow flames presented here, the Zeldovich number and the heat release parameter are held constant. The important relation which is retained is that $\tau_c \propto B^{-1}$. This study is described in section 4 after a review of results found in edge flames.

3. Review of dimensional analysis of edge flames

Now that the pertinent dimensionless parameters have been defined, one can review results obtained for edge flames. In a classical paper, Marble and Adamson [3] used analytical methods derived for the study of boundary layers to analyse stabilization in a laminar mixing zone between premixed reactants and a stream of hot gases at different temperatures. They pose two questions that remain central to future work: do the reactants ignite? If so, how far downstream of the splitter plate does ignition occur? From calculations of the temperature profile across the mixing layer, it is judged that ignition has occurred when the maximum temperature has exceeded the inlet temperature of the hotter stream. This is shown in figure 3(a). This analysis gives a single solution which is valid over all length scales. The reactants always ignite, although the distance over which this occurs can be extremely large. The analytical expression derived for the flame stand-off distance is complicated but it can be rearranged in the following form:

$$L_c = \eta_i^2 \; U_2 \; \tau_c \; \exp\left\{\frac{T_a}{T_2}\right\} \; \{\mathcal{O}(1)\} \tag{9}$$

The value of η_i is approximately constant. Subscript '2' refers to the hot stream. When expressed in terms of the non-dimensional parameters introduced for the cross-flow flame, which are equally valid for edge flames, this leads to an approximate expression:

$$\Pi \propto \mathrm{Da}_2^{-1} \exp\left\{\frac{T_a}{T_2}\right\} \tag{10}$$

The stand-off distance depends on the inverse of the Damköhler number and is a strong function of the Zeldovich number defined with respect to the temperature of the hotter reactant.

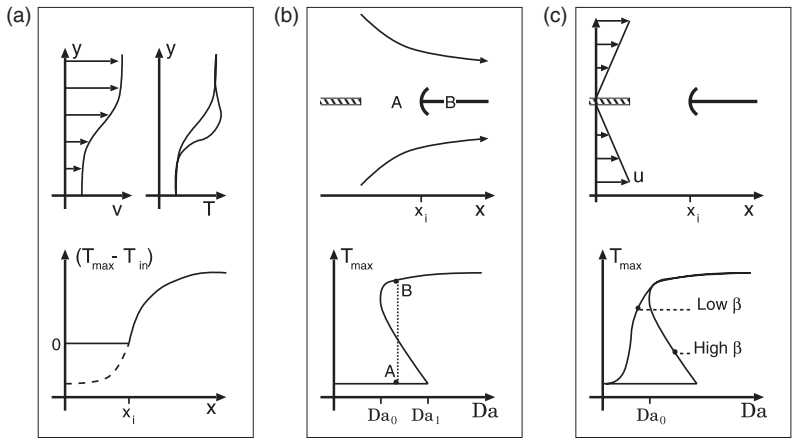

Figure 3. Three approaches to the modelling of edge flames. (a) Marble and Adamson [3] study a laminar mixing layer between premixed reactants and hot combustion products. They consider that ignition occurs when the temperature in the mixing layer first exceeds the inlet temperature of the hotter stream. This model predicts a smooth transition from cold flow to a stable flame in all situations. (b) Buckmaster [4] studies the flow behind a splitter plate in uniformly accelerating flow. Ignition is regarded as corresponding to a sudden jump from state A to state B on the S-shaped diagram. (c) Fernández and Liñan [9] study the third configuration, which is found to exhibit either a smooth transition or a sudden jump to combusting flow depending on a Zeldovich number: $Ze = T_a/T_f$. Smooth transition corresponds to the S-shaped curve which does not double back on itself.

This feature is also found for ignition times in counterflow diffusion flames formed between hot and cold reactant streams [19].

A similar problem is somewhat differently examined in [4]. Conditions prevailing in steady diffusion flames can be characterized by a Damköhler number, as shown in the S-shaped curve in figure 3(b). This behaviour is seen very clearly in one-dimensional counterflow diffusion flames [20]. Solutions along the bottom branch correspond to premixing with negligible reaction. Solutions along the top branch correspond to a thin and highly exothermic flame. The central part corresponds to unstable solutions which are never seen in practice. These authors envisage an edge flame as the transition of a flow from a solution at point A on the bottom branch to a solution at point B on the top branch. This transition occurs at a point in space which can move upstream or downstream, depending on inlet conditions.

The model presented in [4] contains two-dimensional features, as shown in figure 3(b). The edge flame is situated in an accelerating flow ($u = Ax$) and loses heat by diffusion on both sides. By crudely modelling this latter feature the flow is reduced to a one-dimensional form. There are no solutions for Da $<$ Da_0, two solutions for Da_0 $<$ Da $<$ Da_1 and one solution for Da $>$ Da_1. Thus, this model accounts for the top and middle branches of the S-shaped curve. Only the extinct solution can exist below Da_0, so the reactants cannot ignite under these conditions.

Note that this approach is physically distinct from that in [3], where there is a continuously increasing reaction rate along the interface between the two reactants. A single solution is obtained, which means that if the results are presented in terms of a Damköhler number, the response will not be multi-valued.

The edge flame directly behind an infinitely thin splitter plate is considered in figure 3(c) [9]. Boundary layers with uniform strain rate are modelled by imposing the velocity profile $u = A|y|$, where y is the vertical distance from the plate. It is found that the Damköhler number $\mathrm{Da} \equiv s_L \mathcal{D}^{-1/2} A^{-1/2}$ is influential in determining the structure of the flow. Here, s_L is the laminar burning velocity, which scales with $\mathcal{D}^{1/2} \tau_c^{-1/2}$. This Damköhler number is therefore equivalent to Da_1 defined for the strain-rate controlled cross-flow flame.

The Zeldovich number is defined as $Ze \equiv T_a(T_f - T_{\mathrm{in}})/T_f^2$ in [9]. At $Ze > 10$ it is found that three solutions exist above a critical value of Da (Da_0): the frozen solution, the unstable solution and the strong flame solution. This is exactly the development described in [4] relating to the S-shaped curve in figure 3(b). The flame edge is close to the splitter plate for high values of Da but blows off suddenly below Da_0. On the other hand, at $Ze < 10$, a single solution exists. In other words the S-shaped curve no longer doubles back on itself and the behaviour described by the model in [3] is recovered. In this case, a flame kernel forms which moves smoothly away from the splitter plate as the Damköhler number decreases. It eventually becomes a triple flame because the premixed region forming in front of the flame becomes large compared with the diffusion flame thickness.

The results of [9] are obtained mainly in the thermodiffusive limit, where modification of the flow field by heat release is ignored. In [1, 21] it is maintained that this modification must be taken into account in order to determine the flame-holding mechanism. In simulations outside the thermodiffusive limit [9], Da_0 decreases as the heat release parameter is increased. This demonstrates the destabilizing nature of thermal expansion within the reaction kernel and concurs with the findings of [1]. However, a detailed examination of the effect of the heat release parameter is not performed in these references.

In summary, previous work on edge flames highlights the role of the Damköhler number in determining the stand-off distance. The Zeldovich number seems to cause a qualitative change in the stabilization mechanism. The heat release parameter is destabilizing but this is less well documented.

4. Effect of Damköhler number on a cross-flow flame

In this study of cross-flow flames, only the role of the Damköhler number is investigated. The roles of the Zeldovich number and the heat release parameter, which are mostly inherent to the properties of the reactants, are left for further work. Reference [9] defines the Zeldovich parameter as $Ze \equiv T_a(T_f - T_{\text{in}})/T_f^2$. By this definition, Ze lies between 2.7 and 4.4 in the situations under investigation here. This is below $Ze = 10$, where a qualitative change in behaviour occurs, and represents well the properties of most fuels. The heat release parameter is approximately 0.6 for the strain rate-controlled flame and 4 for the convection-controlled flame.

A numerical platform is developed and results validated against direct numerical simulations of a cross-flow flame available in the literature. Numerous simulations are then performed over a wide range of operating conditions in order to determine the relation between the dimensionless parameters Π and Da for the strain-rate- and convection-controlled flames.

4.1. Description and validation of numerical platform

The model problem of a cross-flow flame found in [1] is taken as a reference case. Two codes were used in this reference, both with single-step chemistry:

- The DNS code NTMIX, which is described in [22, 23]. (The acronym NTMIX has no particular meaning.) This code is sixth order in space and third order in time. The compressible Navier–Stokes equations (mass, momentum and energy expressed in terms of temperature) are integrated over a square domain together with transport equations for fuel, oxidizer and product mass fractions.
- The ThermoDiffusive Flow solver (TDF) code, which is formulated in the thermodiffusive limit was originally developed in [19]. The density is kept constant in these calculations and the transport equations for species are decoupled from the Navier–Stokes equations. It is then possible to specify the flowfield and calculate the species distributions.

The TDF code requires considerably less CPU time than the DNS code. However, it cannot simulate modification of the flow by heat release. The DNS code can only deal with simple rectangular geometries, uses a uniform mesh and requires a large amount of CPU time to converge to a steady solution because it uses an explicit time integration scheme. Because the interest is in steady-state solutions one may use an alternative scheme which is less time consuming. The Navier–Stokes equations are solved with second order implicit schemes included in the Fluent software package. This solution is developed on an unstructured mesh, which can be changed during convergence if necessary. The flow solver is optimized for workstations and requires less CPU time to achieve convergence than the thermodiffusive code. The solver in the corner flame configuration, with the flame model defined below, is designated FSP.

In order to validate FSP against the DNS results, the test case of [1] is repeated. NTMIX is a dimensionless code, while FSP is dimensional, so care is required when comparing the two. Thermochemical constants and rate expressions are gathered in table 2 for both codes. Oxidizer enters from the bottom boundary and fuel from the left. The flow exits through the top and right boundaries, where a linear term $\sigma(p - p_a)$ is included in the boundary condition to force the pressure towards the ambient value (σ is a pressure relaxation parameter, see [16]). The inlet profiles are given in table 3. The domain is square with sides of $L_{\text{ref}} = 0.72\,\text{mm}$ in NTMIX and 1.0 mm in FSP. In the test case, $U = V = 6.94\,\text{ms}^{-1}$ and $a = 2.78 \times 10^3\,\text{m}^{-1}$, where a characterizes the steepness of the hyperbolic tangent velocity profile at the origin. U and V are the free stream velocities entering the left and bottom boundaries respectively.

Table 2. Thermochemical constants and rate expressions for the numerical test case, which is performed on two numerical platforms: NTMIX and FSP.

NTMIX		
Reaction	$\mathrm{F} + s\mathrm{O} \rightarrow (1+s)\mathrm{P}$	$s = 1$
Reaction rate	$\dot{w}_T$	$B(\rho Y_F)(\rho Y_O)\exp(-(T_a/T))$
Pre-exponential factor	B	$1 \times 10^{15}\ \mathrm{m^5\,kg^{-1}\,s^{-3}}$
Activation temperature	T_a	8000 K
Heat release (/kg fuel)	q	$2.26 \times 10^6\ \mathrm{J\,kg^{-1}}$
Inlet temperature	T_{in}	1200 K
Molar masses	W_O, W_F, W_P	Not required
Heat capacity	c_p	$965.8\ \mathrm{J\,kg^{-1}\,K^{-1}}$
FSP		
Reaction	$\mathrm{F} + s\mathrm{O} \rightarrow (1+s)\mathrm{P}$	$s = 1$
Molar reaction rate	$-\dot{w}_F = k$	$B[\mathrm{F}][\mathrm{O}]\exp(-(T_a/T))$
Pre-exponential factor	B	$8.85 \times 10^9\ \mathrm{m^3\,kmol^{-1}\,s^{-1}}$
Activation temperature	T_a	8000 K
Heat release (/kmol fuel)	q	$q = 4.52 \times 10^7\ \mathrm{J\,kmol^{-1}}$
Inlet temperature	T_{in}	1200 K
Molar masses	W_O, W_F, W_P	$20\ \mathrm{kg\,kmol^{-1}}$
Heat capacity	c_p	$965.8\ \mathrm{J\,kg^{-1}\,K^{-1}}$
Both		
Viscosity	μ	$1.55 \times 10^{-7} T^{0.76}\ \mathrm{N\,sm^{-2}}$
Thermal diffusivity	λ	$8.26 \times 10^{-4} T^{0.76}\ \mathrm{W\,m^{-1}\,K^{-1}}$
Mass diffusivity	$\mathcal{D}$	$2.41 \times 10^{-9} T^{1.76}\ \mathrm{m^2\,s^{-1}}$

Table 3. Boundary conditions for the test case of a cross-flow flame. In the limit $ax \rightarrow 0$ the flame is strain-rate controlled. In the limit $ax \rightarrow \infty$ the flame is convection controlled.

Bottom boundary			Left boundary		
General expression	$\lim_{ax\to 0}$	$\lim_{ax\to\infty}$	General expression	$\lim_{ax\to 0}$	$\lim_{ax\to\infty}$
$v = U\tanh(ax)$	$v = (aU)x$	$v = U$	$v = 0$	$v = 0$	$v = 0$
$u = 0$	$u = 0$	$u = 0$	$u = U\tanh(ax)$	$u = (aU)x$	$u = U$
$Y_O = \tanh(ax)$	$Y_O = ax$	$Y_O = 1$	$Y_O = 0$	$Y_O = 0$	$Y_O = 0$
$Y_P = 1 - \tanh(ax)$	$Y_P = 1 - ax$	$Y_P = 0$	$Y_P = 1 - \tanh(ax)$	$Y_P = 1 - ax$	$Y_P = 0$
$Y_F = 0$	$Y_F = 0$	$Y_F = 0$	$Y_F = \tanh(ax)$	$Y_F = ax$	$Y_F = 1$

The volumetric heat release rate and temperature fields obtained from both codes are shown in figure 4. The contours nearly coincide, although FSP gives a lower volumetric heat release rate and a lower temperature than NTMIX. There are various possible reasons for the difference:

- Numerical diffusion is greater for FSP (second order in space) than for NTMIX (sixth order in space).
- The thermochemical models do not match exactly.

In addition, both codes force the contour lines to tend towards being normal to the exit boundaries. In figure 4 this effect can only be seen in the NTMIX results because only part of the computational domain of the FSP code is shown.

In conclusion, the results of FSP are sufficiently close to the results of NTMIX that it can be used with confidence. It solves the full Navier–Stokes equations and can therefore take into

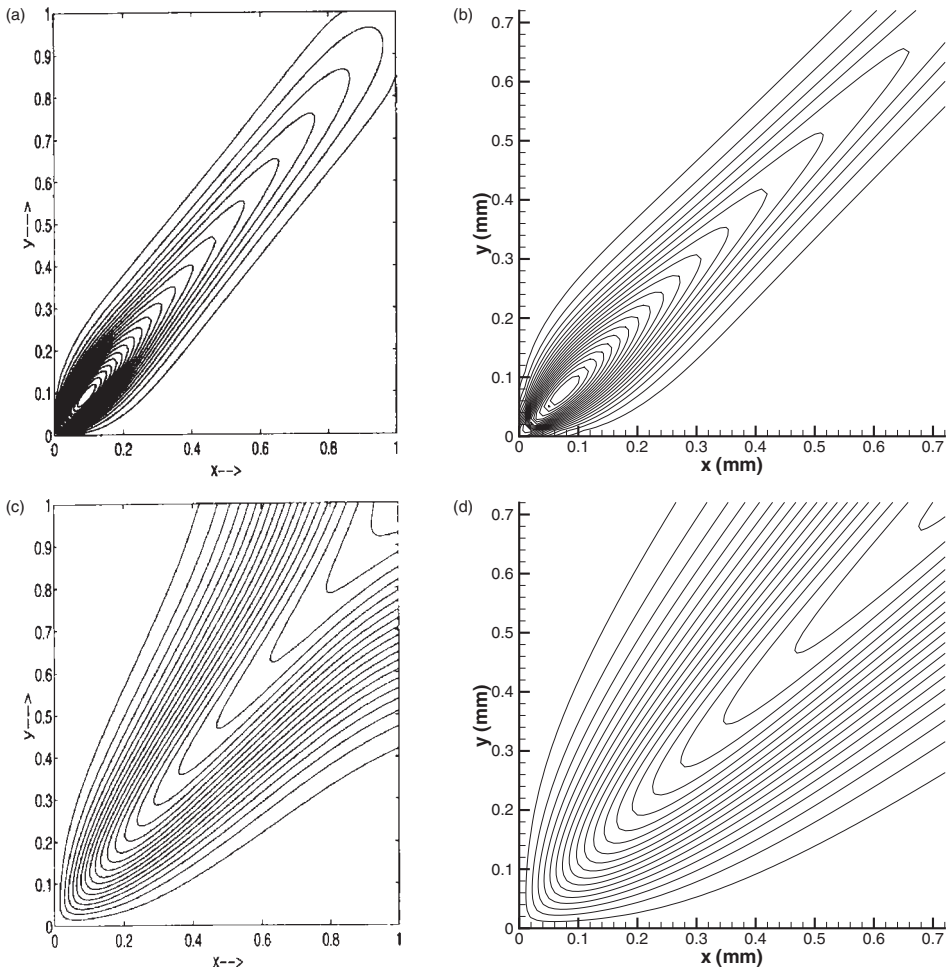

Figure 4. Contours of volumetric heat release rate, $\dot{q}_v$, and temperature, T, for the test case in section 4.1. Results of NTMIX, from Mahalingam *et al* [1], are given on the left. Results of FSP are shown on the right. (*a*) Contours of heat release rate. Maximum value $3.0 \times 10^{10}\,\mathrm{J\,m^{-3}\,s^{-1}}$, NTMIX, $L_{\mathrm{ref}} = 0.72\,\mathrm{mm}$. (*b*) Contours of heat release rate. Maximum value $1.5 \times 10^{10}\,\mathrm{J\,m^{-3}\,s^{-1}}$, calculated with FSP. (*c*) Contours of temperature. Maximum value 2244 K, NTMIX, $L_{\mathrm{ref}} = 0.72\,\mathrm{mm}$. (*d*) Contours of temperature. Maximum value 2080 K, calculated with FSP.

account the effect of heat release on the velocity field. The CPU time required is at least an order of magnitude smaller than that required by NTMIX, which makes it well suited for a parametric study.

4.2. Strain-rate-controlled flame

Entry velocity profiles for the strain-rate-controlled flame are shown in figure 5 with a typical solution. Species inlet profiles are flat. The domain is otherwise the same as the test case in section 4.1.

The chemical time τ_c is proportional to the inverse pre-exponential factor B^{-1}, which is varied by a factor of 64. A and $\mathcal{D}$ are both varied by a factor of 256 in various combinations with B. The molecular diffusivities λ and ν are altered such that $Le = Pr = 1$. Each

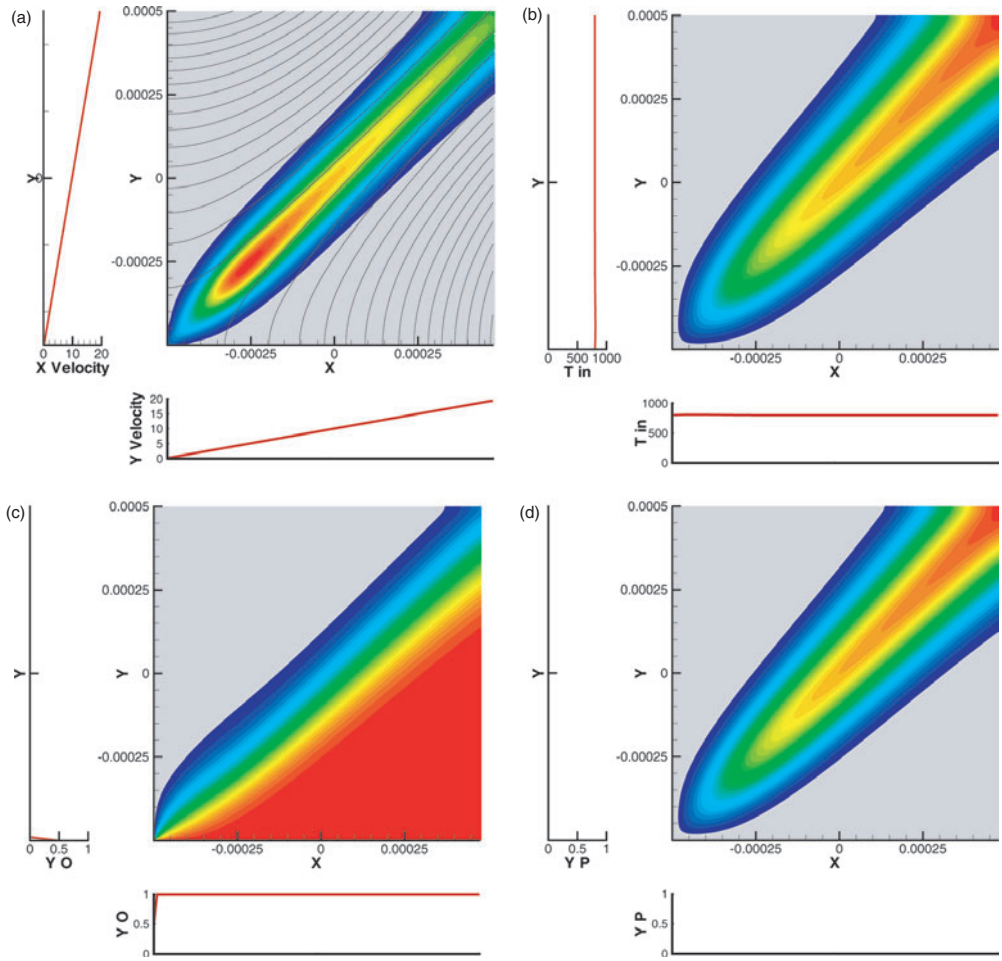

Figure 5. Strain-rate-controlled cross-flow flame. Oxidizer enters from the bottom boundary and fuel from the left. Inlet profiles are shown next to the main field. The inlet velocity profiles follow $u = Ay$ and $v = Ax$. The inlet temperature (900 K) is high enough for the reactants to react on contact. The grid was refined in the corner to check that flame-holding was not numerical. (*a*) Volumetric heat release rate, maximum value $= 9.4 \times 10^9$ W m^{-3}, and streamlines. (*b*) Temperature, maximum value = 1760 K. (*c*) Mass fraction of oxygen. (*d*) Mass fraction of products.

of the 130 individual simulations provides the flame stand-off distance L_c, defined as the distance from the corner to the position of highest reaction rate. This is expressed as a multiple of the flame thickness. The relatively coarse grid size (200 × 200 cells) means that these simulations are only valid over a limited range of L_c/δ_f. This can be estimated as follows: a fat flame close to the corner is limited by the bottom and left boundaries such that $L_c/\delta_{f\,(\mathrm{min})} \approx 2$, as shown in figure 6(*a*). On the other hand a thin flame far from the corner, such as that in figure 6(*b*), is limited by the grid size: $L_c/\delta_{f\,(\mathrm{max})} \approx 200/10 = 20$. This valid range corresponds to $10 < \Pi < 100$ because for the material properties in use here, $\tau_c^{1/2}\mathcal{D}^{1/2} \approx 5\delta_f$. In addition, above a reduced stand-off distance $\Pi = 30$, the flame spans only a few gridpoints, leading to artificially high numerical diffusivity. This leads to artificially large values of Π because there is a hidden increase in $\mathcal{D}$. Results in the valid region are plotted in figure 7 with Π as a function of Da_1. It is clear that $\Pi \propto \mathrm{Da}_1^{-2}$. This correlation does not

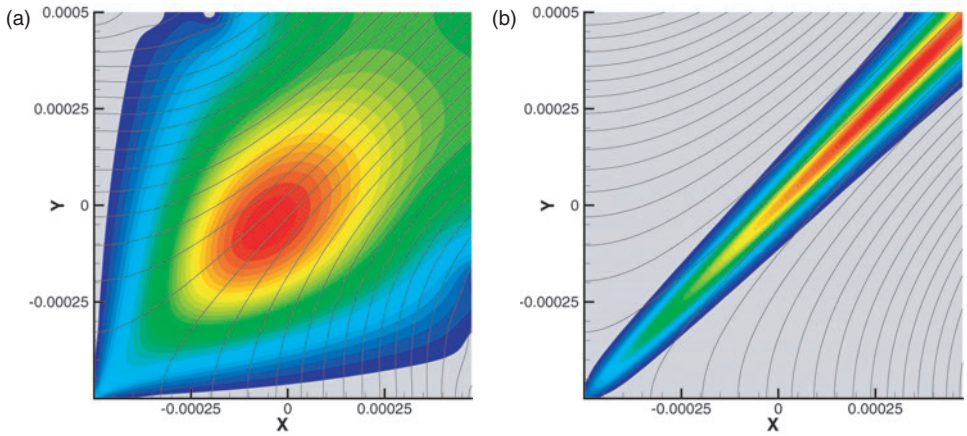

Figure 6. The numerical simulations are only valid within a certain range of L_c/δ_f due to the size of the grid relative to the domain. This valid range is estimated to correspond to $100 < \Pi < 10$. However, the results suggest that the true valid range is closer to $30 < \Pi < 10$, probably due to artificially high numerical diffusivity inherent in the numerical platform when the flame spans only a few grid points. (*a*) L_c/δ_f limited by size of domain. (*b*) L_c/δ_f limited by size of grid.

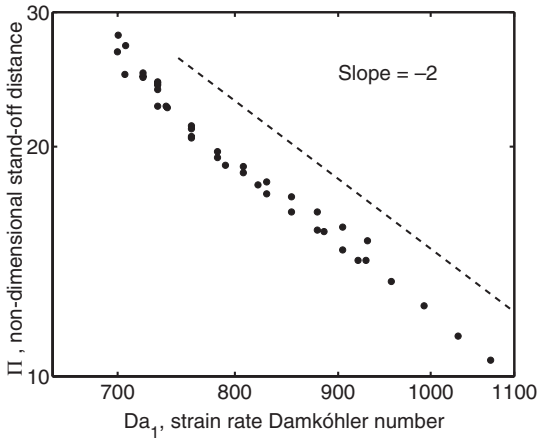

Figure 7. Non-dimensional stand-off distance, $\Pi = L_c\,\tau_c^{-1/2}\,\mathcal{D}^{-1/2}$, plotted as a function of the strain rate Damköhler number, $\mathrm{Da}_1 = A^{-1/2}\,\tau_c^{-1/2}$, for a flame in a corner. Above $\mathrm{Da}_1 = 700$ this follows the relation: $\Pi \propto \mathrm{Da}_1^{-2}$.

arise simply because τ_c appears in both parameters. If this were the case, the exponent would be 1 because both parameters have the same dependence on τ_c. This leads to:

$$L_c \propto A\,\mathcal{D}^{1/2}\,\tau_c^{3/2} \tag{11}$$

The stand-off length increases as the strain rate, A, increases. It decreases rapidly as the chemical time decreases. These features are to be expected. It is slightly curious that L_c increases when the diffusivity increases because this would usually increase the propagation speed of the flame kernel. However, in this case increasing $\mathcal{D}$ also increases the rate at which heat drains to the inlet boundaries. Since the incoming streams are held at a fixed temperature in this model, this energy is lost. This feature is similar to the fixed temperature boundary condition of a condensed fuel.

4.3. Convection-controlled flame

The test case in section 4.1 is adapted to create a convection-controlled environment and the species inlet profiles are made flat. The domain and velocity inlet profiles are shown in figure 8 with an example of a solution.

The chemical time τ_c is proportional to the inverse pre-exponential factor B^{-1}, which is varied by four orders of magnitude. The injection velocity U and diffusivity $\mathcal{D}$ are both varied by three orders of magnitude in various combinations with B. The coefficients λ and ν are altered such that $Le = Pr = 1$. In each of the 100 simulations, the flame stand-off distance L_c is measured. This quantity is defined as the distance from the corner to the position of highest reaction rate. The simulations only give reasonable solutions over the range of $\Pi = L_c/\delta_f$ to which the computational domain is well adapted. At high Π the flame becomes too thin to be resolved by the mesh. At low Π the flame is very thick and is strongly affected by the boundary conditions, which are somewhat artificial. The results are plotted in figure 9 with Π as a function of Da_2. In the valid range, which corresponds here to $10 < \Pi < 100$, the points

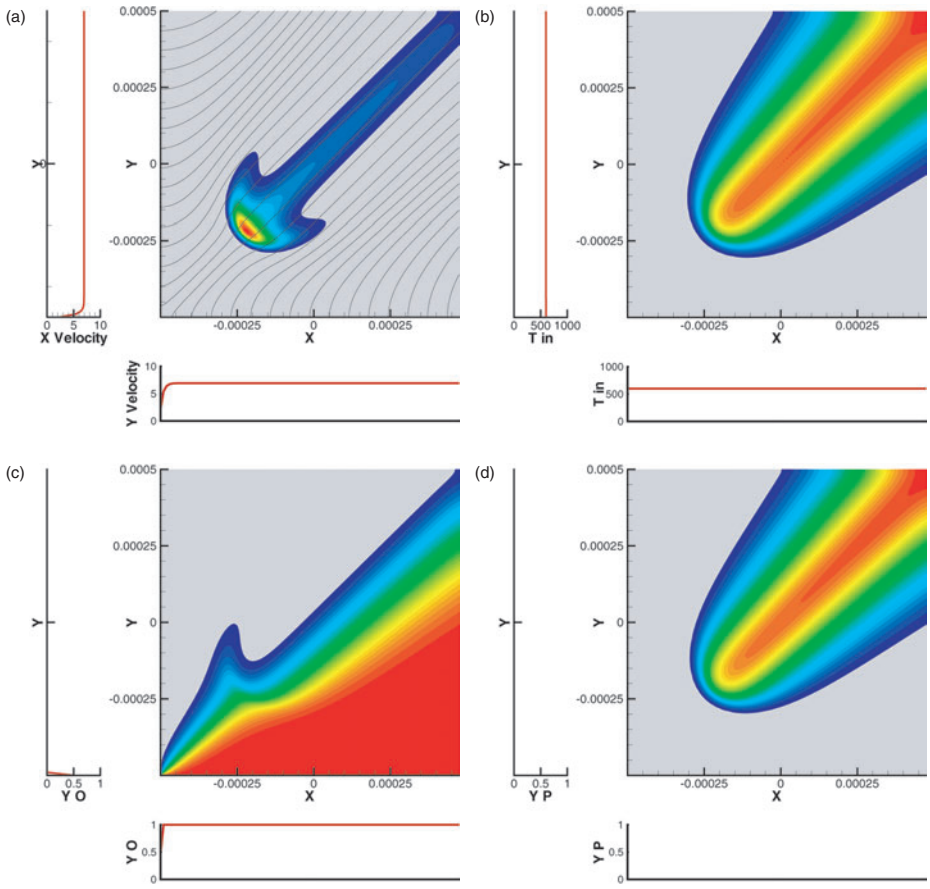

Figure 8. Convection-controlled diffusion flame in a corner. Oxidizer enters from the bottom, fuel from the left. Inlet profiles are shown next to the main field. The inlet temperature is 600 K. (*a*) Volumetric heat release rate, maximum value $= 1.4 \times 10^{11}$ W m^{-3}, and streamlines. (*b*) Temperature, maximum value $= 3022$ K. (*c*) Mass fraction of oxygen. (*d*) Mass fraction of products.

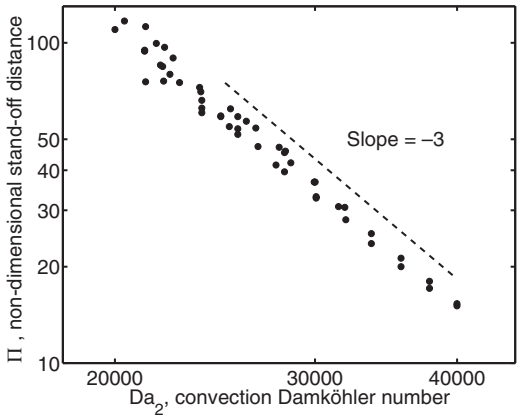

Figure 9. Non-dimensional stand-off distance, $L_c\,\tau_c^{-1/2}\,\mathcal{D}^{-1/2}$, as a function of the convection Damköhler number, $\mathcal{D}^{1/2}\,U^{-1}\,\tau_c^{-1/2}$, for a flame in a corner.

collapse to the same line, which obeys the relation: $\Pi \propto \mathrm{Da}_2^{-3}$. This leads to:

$$L_c \propto U^3\,\tau_c^2\,\mathcal{D}^{-1} \tag{12}$$

This can also be written as $L_c \propto (U/s_L)^2 U\,\tau_c$. The stand-off length is a strong function of the flow velocity, as would be expected for a convection-controlled flame. The stand-off distance reduces when $\mathcal{D}$ increases because the speed of the flame kernel increases. Interestingly, $\Pi \propto \mathrm{Da}^{-1}$ for an edge flame formed between parallel reactants [3]. This demonstrates that the cross-flow flame is significantly more sensitive to the inlet velocity than an edge flame.

5. Conclusion

Two types of cross-flow flames are investigated in this paper. The first are formed in a field of constant strain rate while the second are convection controlled. Dimensional analysis is used to highlight the parameters that describe the stand-off distance of such flames. By examining edge flames, which are closely related, the Damköhler number is revealed as the most influential of these. The Zeldovich number and the heat release parameter will be the subject of future study. A numerical approach is used to determine the effect of the Damköhler number. One can conclude that, for the strain-controlled flame, the dimensionless stand-off distance $\Pi \propto \mathrm{Da}^{-2}$, leading to a scaling law: $L_c \propto A\,\mathcal{D}^{1/2}\,\tau_c^{1/2}$, where A is the strain rate, $\mathcal{D}$ is the diffusivity and τ_c is the chemical time. Similarly, for the convection-controlled flame, the dimensionless stand-off distance $\Pi \propto \mathrm{Da}^{-3}$, leading to: $L_c \propto U^3\,\tau_c^2\,\mathcal{D}^{-1}$, where U is the injection velocity. Cross-flow flames are much more sensitive to the Damköhler number than are edge flames, for which $\Pi \propto \mathrm{Da}^{-1}$. The existence of solutions for cross-flow or corner flames, reported in [17], suggests that comparisons with work of the present kind may be profitably pursued.

Acknowledgments

This work has been supported by CNES and Snecma as part of the research group ‘Combustion in Rocket Engines’.

References

[1] Mahalingam S, Thevenin D, Candel S and Veynante D 1999 Analysis and numerical simulation of a nonpremixed flame in a corner *Combust. Flame* **118** 221–32

[2] Takahashi F, Schmoll W and Katta V 1998 Attachment mechanisms of diffusion flames *Proc. Combust. Inst.* **27** 675–84

[3] Marble F and Adamson T 1954 Ignition and combustion in a laminar mixing zone *Jet Propulsion* **24** 85–94

[4] Buckmaster J and Weber R 1996 Edge flame holding *Proc. Combust. Inst.* **26** 1143–9

[5] Buckmaster J 1997 Edge-flames *J. Eng. Math.* **31** 269–84

[6] Buckmaster J and Jackson T 2000 Holes in flames, flame-isolas, their edges *Proc. Combust. Inst.* **28** 1957–64

[7] Higuera F and Liñán A 1996 Flow field of a diffusion flame attached to a thick-walled injector bandween two coflowing reactant streams *J. Fluid Mech.* **329** 389–411

[8] Deshpande M, Venkateswaran S, Foust M and Merkle C 1997 Finite splitter plate effects on flame holding in a confined hydrogen–oxygen shear layer *35th Aerospace Sciences Meeting and Exhibit*—AIAA Paper 97-0258

[9] Fernández E, Kurdyumov V and Liñán A 2000 Diffusion flame attachment and lift-off in the near wake of a fuel injector *Proc. Combust. Inst.* **28** 2125–31

[10] Hirano T and Kanno Y 1973 Aerodynamic and thermal structures of the laminar boundary layer over a flat plate with a diffusion flame *Proc. Combust. Inst.* **14** 391–8

[11] Williams F 1985 *Combustion Theory* (New York: Benjamin/Cummings)

[12] de Ris J 1969 Spread of a laminar diffusion flame *Proc. Combust. Inst.* **12** 241–52

[13] Chorpening B, Knott G and Brewster M 2000 Flame structure and burning rate of ammonium perchlorate/hydroxyl-terminated polybutadiene propellant sandwiches *Proc. Combust. Inst.* **28** 847–53

[14] Herding G, Snyder R, Scouflaire P, Rolon C and Candel S 1996 Flame stabilization in cryogenic propellant combustion *Proc. Combust. Inst.* **26** 2041–7

[15] Emmons H 1956 The film combustion of liquid fuel *Z. Angew. Math. Mech.* **36** 60–71

[16] Poinsot T and Veynante D 2001 *Theoretical and Numerical Combustion* (Philadelphia, PA: Edwards), pp 426–7

[17] Mahalingam S and Weidman P 2002 Activation energy asymptotics analysis and numerical modelling of a strained laminar corner flame *Combust. Theory Modelling* **6** 155–72

[18] Weller A 1955 Similarities in combustion—a review *Selected Combustion Problems* ed M Thring (London: Butterworths)

[19] Thévenin D and Candel S 1994 Ignition dynamics of a diffusion flame rolled up in a vortex *Phys. Fluids* **7** 434–45

[20] Darabiha N 1992 Transient behaviour of laminar counterflow hydrogen–air diffusion flames with complex chemistry *Combust. Sci. Technol.* **86** 163–81

[21] Hirano T and Kinoshita M 1975 Gas velocity and temperature profiles of a diffusion flame stabilized in the stream over liquid fuel *Proc. Combust. Inst.* **15** 369–87

[22] Baum M, Poinsot T, Haworth D and Darabiha N 1994 Using direct numerical simulations to study $H_2/O_2/N_2$ flames with complex chemistry in turbulent flows *J. Fluid Mech.* **281** 1–32

[23] Poinsot T, Candel S and Trouvé A 1996 Direct numerical simulation of premixed turbulent combustion *Prog. Energy Combust. Sci.* **21** 531–76